Iranian Journal of Pharmaceutical Sciences
2026: 22 (1): 46- 66
https://journals.sbmu.ac.ir/IJPS

Research Article

OPEN ACCESS

AI-Driven Discovery of Syringic Acid as an Anthelmintic Agent: Integrating PySCF-Based DFT, Molecular Dynamics, and In Vitro Validation Targeting β-Tubulin

Hanumanthappa Makari[a], Prasanth D S N B K [b*], Praveen Kumar Pasala[c], Deepak A Yaraguppi[d], Tummala Anusha [e], Haindavi Borra [f], Lakshmi Chandana Kanamarlapudi [f], Esritha Tallapaka [f]

[a] *Department of Biotechnology, Maharani's Science College for Women (Autonomous), Mysuru- 570005, Karnataka, India.*
[b] *School of Pharmacy & Technology Management, SVKM's Narsee Monjee Institute of Management Studies (NMIMS), Polepally SEZ, TSIIC, Jadcherla, Mahbubnagar, Hyderabad, 509301, India.*
[c] *Raghavendra Institute of Pharmaceutical Education and Research, JNTUA, Anantapuramu, Andhra Pradesh 515721, India.*
[d] *Department of Biotechnology, KLE Technological University, Hubli, Karnataka 580031, India.*
[e] *Electroanalytical Lab, Department of Chemistry, Koneru Lakshmaiah Education Foundation, Vaddeswaram, Guntur, Andhra Pradesh 522302, India.*
[f] *Department of Pharmacognosy, KVSR Siddhartha College of Pharmaceutical Sciences, Vijayawada - 520010, Andhra Pradesh, India.*

Received: August 12, 2025 **Last Revision:** October 14, 2025 **Accepted:** October 28, 2025 **Available online:** January 27 2026.

Abstract

Helminthiasis is a global health issue that is particularly prevalent in developing countries. Current anthelmintic drugs, mainly benzimidazoles, have side effects and are resistant to parasites. This study investigated the anthelmintic activity of syringic acid (SYR), a natural polyphenolic compound, against Pheretima posthuma, which targets β-tubulin, using both in silico and in vitro approaches. Drug likeness and ADME/T showed that SYR has a better pharmacokinetic profile than albendazole (ALB). Density functional theory calculations provided insight into the electronic properties and reactivity of SYR and ALB. Molecular docking studies revealed that SYR has a strong binding affinity (ΔG = -6.3 kcal/mol) for β-tubulin, similar to that of ALB (ΔG = -7.2 kcal/mol). Molecular dynamics simulations confirmed the stable binding of SYR in the β-tubulin active site for 100 ns. *An* in vitro anthelmintic assay on Pheretima posthuma demonstrated that SYR exhibits dose-dependent activity in inducing paralysis and mortality, but is less potent than ALB. The consistency between the computational predictions and empirical bioactivity assays provided preliminary evidence that SYR is a genuine anthelmintic agent. However, further in vivo studies are needed to evaluate the pharmacodynamics, safety, and immunological effects of SYR in complex biological systems before clinical trials. This study provides a basis for the development of new, safer, and more effective anthelmintic agents that target β-tubulin, addressing the problems associated with drug resistance and the side effects of current treatments.

Keywords: Syringic acid; Anthelmintic; In silico; β-*Tubulin*; In vitro; *Pheretima posthuma.*

1. Introduction

Helminthiasis is a severe health burden worldwide on a large scale, and the discovery of new anthelmintics is seriously handicapped by increasing resistance to existing drugs such as albendazole (ALB) and by the long duration and high cost of conventional drug discovery [1]. This study hypothesizes that syringic acid (SYR; 4-hydroxy-3,5-dimethoxybenzoic acid), a

*** Corresponding Author**:
D S N B K Prasanth, School of Pharmacy & Technology Management, SVKM's Narsee Monjee Institute of Management Studies (NMIMS), Polepally SEZ, TSIIC, Jadcherla, Mahbubnagar, Hyderabad, 509301, India.. E-mail: dsnbkprasanth@gmail.com.

Cite this article as: Makari H., D S N B K. P., Pasala P. K., Yaraguppi D.A., Anusha T., Borra H., Kanamarlapudi L. Ch., Tallapaka E. AI-Driven Discovery of Syringic Acid as an Anthelmintic Agent: Integrating PySCF-Based DFT, Molecular Dynamics, and In Vitro Validation Targeting β-Tubulin. Iran. J. Pharm. Sci., 2026, 22 (1): 46- 66.

DOI: https://doi.org/10.22037/ijps.v22i1.49733

naturally occurring phenolic compound, is a promising anthelmintic candidate against β-tubulin. We further suggest that an AI-integrated workflow combining DFT, molecular docking, dynamics, and in vitro-based validation helps to derisk novel drug candidates in a fast and efficient manner. The choice of SYR was based on its good drug-like properties, antioxidant and anti-inflammatory potential, which could offer additional benefits [2], and the known bioactivity of structurally related syringyl derivatives, such as the proteasome inhibitor syringolin A, implying unexplored therapeutic avenues.

To validate this hypothesis, we targeted a very well-established eukaryotic cytoskeletal element, β-tubulin, which is essential for helminth cell division, motility, and structural integrity [3]. Benzimidazoles are efficacious against this target; however, point mutations in the β-tubulin gene that affect the drug-binding site reduce their drug action. Hence, there is an urgent need to identify agents that can overcome such resistance mechanisms either by interacting with alternative binding sites or through alternative conformations.

According to the World Health Organization (WHO), helminthic infections pose a significant global health burden, are concentrated mainly in tropical and subtropical regions, and affect and afflict more than a billion people [4]. These parasitic diseases are significant contributors to human morbidity, causing malnutrition, impairing cognitive development, and reducing economic productivity. An increasing number of anthelmintics have lost their efficacy over time because of the development of older off-label resistance. For example, resistance to many conventional anthelmintics is increasing, and some others are deterred from use owing to their severe toxicity or lack of broad interspecies spectrum activity (2). This calls for the discovery of newer agents that would be comparatively more efficacious, along with better safety profiles and mechanisms of action.

The traditional drug discovery pathways are time-consuming and resource-intensive, and are typically characterized by high attrition rates. The approach to faster identification and optimization of bioactive compounds stems from integrating advanced computational methodologies, particularly those that utilize artificial intelligence. Screening platforms based on AI can operate efficiently across any space to predict the first possible drugs and drug-target interactions. The most powerful method for understanding and simulating molecular recognition and binding kinetics is the association of these AI predictions with quantum chemical calculations, such as density functional theory, or the calculation of dynamic simulations, such as molecular dynamics. This computational framework, combined with rigorous in vitro validation, provides a smoother and cost-effective means of anthelmintic development.

Syringic acid (4-hydroxy-3,5-dimethoxybenzoic acid) is a phenolic compound that exists almost unenforcedly in plants. Along with the hydroxyl group and two methoxy groups on the benzene ring, these features bestow upon it its antioxidant and anti-inflammatory actions. While the anthelmintic activity of syringic acid has not been directly described in the literature, closely related syringyl derivatives have been shown to have different uses. For example, syringolin A is a proteasome inhibitor with antiproliferative activity [5, 6]. Syringin has been suggested to ameliorate cardiac hypertrophy [7], and syringaresinol derivatives have demonstrated antidiabetic activities associated with antioxidative properties [8]. A further derivative, syringetin, a flavonoid-based derivative, inhibits osteoclastogenesis [9]. This spectrum of biotransformations suggests the potential for unexplored therapeutic applications of syringic acid, a related phenolic compound.

Compared with αβ-tubulin heterodimers, microtubules represent the major components of the eukaryotic cytoskeleton [10], and in helminths, β-tubulins take part in cell division and motility and maintain structural integrity [11, 12]; hence, they are attractive and validated targets in anthelmintic axes. Tubulin-targeting agents inhibit the polymerization or depolymerization of microtubules [13], with benzimidazoles interacting with β-tubulin to inhibit microtubule assembly. However, resistance often arises from point mutations in the β-tubulin gene, which alter the drug-binding site [14], such as those at amino acid position 350 in Chlamydomonas reinhardtii β-tubulin, which affects sensitivity to inhibitors [15], or cysteine residues such as C354 in yeast β-tubulin, which affect the stability and function of microtubules [16, 17].

Therefore, agents that overcome resistance mechanisms by binding to alternative sites and inducing conformational changes in β-tubulin are urgently needed [18].

Density functional theory (DFT) is a quantum mechanical approach that enables the study of the electronic structure of multiatomic systems, allowing for the accurate prediction of molecular properties and interactions. The PySCF provides a fully flexible structure for DFT computations in Python, allowing electron density, bonding, and energetic landscapes to be analyzed in detail [19-21]. DFT is applied in drug design to study the atomic-level interactions of the ligand with the target protein, specifically β-tubulin, including hydrogen bonds, van der Waals forces, and hydrophobic contacts, with a careful choice of functionals and basis sets to strike a balance between accuracy and computational requirements. PySCF-based DFT calculations elucidate the electronic origin of syringic acid–β-tubulin binding, identify key residues, estimate the energies of interactions, and determine the optimal poses. Such notions form the core of molecular recognition and hence guide lead optimization, as described in the context of colchicine binding to β-tubulin [22, 23]. These findings could therefore be used to devise structural adjustments to syringic acid to increase its affinity for, or specificity to, helminthic β-tubulin variants, which serves as one route toward overcoming resistance.

MD simulations complement DFT by modeling the time-dependent behavior of protein–ligand complexes. They are thus informative about conformational dynamics, induced-fit mechanisms, and the stability of interactions under physiological conditions. In β-tubulin, MD simulations reveal conformational changes in the binding pocket upon syringic acid binding, simultaneously highlighting the flexibility of the ligand within the binding pocket and providing a dynamic view that is absent in static structures [18]. They also enable the estimation of binding free energy, which predicts the stability of binding and the affinity of syringic acid–β-tubulin interactions, while highlighting specific interactions that contribute significantly to binding. This leads to rational modifications of syringic acid to improve its activity, much like in studies on drug interactions at paclitaxel sites or other sites on α-tubulin [24], hence lessening the dependence on extensive synthesis and empirical work.

This high degree of structural and functional conservation of β-tubulin within eukaryotes suggests that β-tubulin may be targeted for anti-helminthic and anti-mitotic drugs. Sequence and structural analyses confirmed that major functional domains, such as the nucleotide-binding region, the Taxol-binding region, and those involved in polymerization, are highly conserved between humans, helminths, and the model organism P. posthuma; this homology thus indicates the potential for P. posthuma to be used as an initial model for the identification of β-tubulin-interacting agents. However, there are considerable limitations in the predictive capacity with respect to translation due to differences in drug-binding residues between species and isotypes, variable expression of isotypes, and differences in the dynamics of microtubules. However, such differences can provide pathways to opposing results between earthworms, parasitic helminths, and human cells, most often making an agent effective in one system and not in another. In essence, P. posthuma may be helpful as a preliminary screen for tubulin-binding activity; however, this should be followed by additional evaluation using either parasite-specific assays or mammalian systems, which may more reliably predict clinical efficacy and specificity [25-27].

This research presents a novel approach to scientifically exploring the broad AI-powered computational-experimental search for new anthelmintic molecules, wherein syringic acid was investigated as a potential tubulin binder. One of the main strengths of the continuous screening platform, which utilizes state-of-the-art AI, DFT calculations within the PySCF environment, and MD simulations, is its ability to assess syringic acid as a candidate of interest while also characterizing its putative interactions with β-tubulin at the atomic and dynamic levels. Further in vitro experiments confirmed that the drug possesses anthelmintic properties, highlighting how computational predictions and experimental observations work in tandem. The conceptual framework presented here provides an important building block for shortening the process of drug discovery, especially in the urgent race against anthelmintic resistance.

2. Materials and methods

2.1. Drug Likelihood and ADME/T Analysis

Employing the DruLito tool, a web-based application, we ascertained the conformity of SYR to drug-like properties based on established parameters. Lipinski's "Rule of Five," a well-recognized framework, was utilized as a primary filter that stipulates that an orally active drug should not violate more than one of the following criteria: no more than five hydrogen bond donors, not exceeding 10 hydrogen bond acceptors, a molecular mass less than 500 Daltons, or an octanol–water partition coefficient (Log P) not greater than five. It was predicted via DruLito software (https://niper.gov.in/pi_dev_tools/DruLiToWeb/DruLiTo_index.html) [28]. An ADME/T integrated profiling study was conducted to identify multidimensional computational platforms that can render the full pharmacological profile of SYR. In particular, specific parameters were attributed to the appropriate tool to leverage the predictive power thereof: SwissADME [29] for physicochemical properties, bioavailability rules, and PAINS alerts; ADMETLAB [30] for absorption, distribution, and cytochrome P450 enzyme inhibition; and ProTox-III [31] for organ toxicity endpoints and LD_{50}. This approach strikes a balance, whereas the limitations and biases inherent in the modalities of any single model are unavoidable.

2.2. Density functional theory (DFT) analysis

In this work, calculations of the electronic properties of SYR and ALB were carried out via DFT at B3LYP/6-311G(d,p) in PySCF 2.10 with RDKit integration[32, 33]. This method was selected due to its acceptance in the study of similar organic systems. While it is possible to apply dispersion corrections to improve the description of noncovalent interactions, the present model was deemed sufficient to describe the intrinsic molecular properties. Geometry optimizations assume tight convergence criteria (change in energy < 1×10^{-6} a.u., max force < 1×10^{-5} a.u./Bohr, RMS displacement < 1×10^{-5} Bohr) and an SCF convergence threshold of 1×10^{-8} a.u. in the gaseous state without invoking an implicit solvent. This gas-phase setup was selected to efficiently compute and compare the intrinsic electronic properties and reactivity descriptors (e.g., HOMO-LUMO energies, electronegativity, and chemical potential) of the isolated molecules. This model does not include dispersion corrections (e.g., Grimme's D3) or implicit solvation, which are necessary for highly accurate quantification of noncovalent binding interactions in a solvated environment. Such advanced calculations are reserved for future studies focused explicitly on interaction energies. The resulting optimized geometries were then used to calculate the absolute values of key parameters, such as the HOMO–LUMO energies, dipole moment, electronegativity, softness, and MEP, without the attachment of any statistical error bars. For visualization purposes, dipole vectors were rendered in PyMOL and Google Colab using Python scripts, with SYA carbons colored violet and ALB carbons pink. In contrast, heteroatoms were identified (O=red, N=blue, S=yellow), with interactive 3D representations generated alongside dipole arrows (scale = 2.0) [34, 35].

2.3. Molecular Docking

The X-ray crystallographic structures of the protein target (β-tubulin) (PDB: 1SA0) were downloaded from the Research Collaboratory for Structural Bioinformatics (RCSB) Protein Data Bank (www.pdb.org) and used as the receptor for the molecular docking experiments (**Figure 1**)[36].

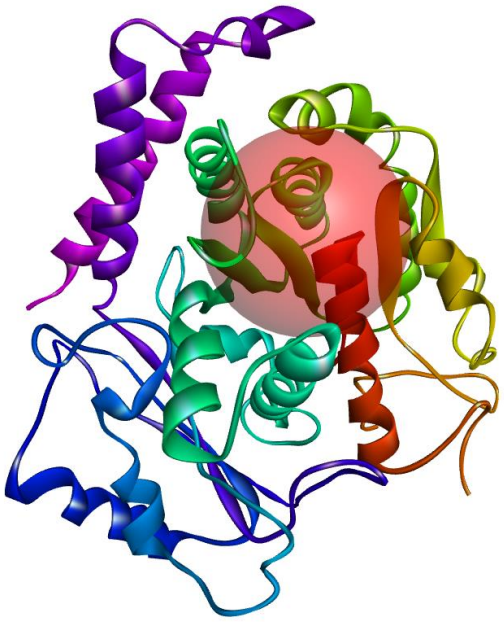

Figure 1: Active pocket of Tubulin-Colchicine: Stathmin-Like Domain Complex (1SA0).

The ligands SYR and standard ALB were downloaded from the PubChem database and converted into PDB via Open Babel software. The random seed was explicitly set to the default value (seed=0) to ensure the reproducibility of the conformational sampling. To conduct virtual screening, the active binding sites of the molecular targets were first determined using the P2RANK server [37, 38], with the other parameters set to their default settings. Molecular docking was performed using AutoDock Vina 1.2.6 software [37]. The grid box was centered on the predicted binding pocket (center_x = 127.224, center_y = 95.792, center_z = 13.062) with dimensions of 15 × 15 × 15 Å and a grid point spacing of 1.0 Å. An exhaustiveness value of 32 was used for the global search algorithm. At the end of docking, the best conformations were analyzed for binding energy (kcal/mol). The conformations with the lowest energy were selected for further analysis. The 2D interactions of the complex protein–ligand structure, including hydrogen bonds and bond lengths, were analyzed via Biovia Discovery Studio software.

2.4. Molecular simulation

Tubulin-colchicine: The Stathmin-like domain complex (1SA0) was chosen as a target for investigation. Docking analysis yielded ALB and SYR. The ligand topology and parameters for SYR were generated via the general AMBER force field (GAFF). Partial atomic charges were assigned via the AM1-BCC method via the Antechamber module of the AmberTools package. The topology for the reference ligand, ALB, was obtained from the ATB server for consistent treatment. We utilized the pdb2gmx module of GROMACS 2025.2 software to introduce hydrogen atoms to the heavy atoms of the system. The prepared systems were initially minimized under vacuum for 1500 steps via the steepest descent algorithm. The structures were subsequently solvated in a cubic periodic box filled with a simple point charge (SPCE) water model. To maintain physiological relevance, the complex systems were balanced with an appropriate salt concentration (0.15 M) by adding the corresponding amounts of Na+ and Cl^- counterions. The system preparation protocol was based on previously published methodologies [38]. Following the NPT equilibration phase, each resulting structure was subjected to a final production run in the NPT ensemble for a simulation time of 100 ns. For all the simulations, the velocity generation step during equilibration used a fixed random seed (old-seed = -1) to ensure reproducible starting conditions. Using the Gromacs tool, we established the trajectory of the protein after the simulation. We performed a trajectory analysis using the root mean square deviation (RMSD), the root mean square fluctuation (RMSF), the radius of gyration (Rg), the solvent-accessible surface area (SASA), and the hydrogen bond pattern (H-bond). To determine the binding free energy of the 1SA0-SYR complex, molecular mechanics Poisson-Boltzmann surface area (MM-PBSA) analysis was performed. The MM-PBSA calculations utilized a solute dielectric constant of 2 and a solvent dielectric constant of 80, with an ionic concentration of 0.15 M and the default mbondi radii set. The GROMACS utility g_mmpbsa was used to estimate the binding free energy. The calculations utilized a solute dielectric constant of 2 and a solvent dielectric constant of 80 to model the electrostatic contributions to solvation. The 1SA0-SYR binding free energy was calculated every 3.31000 frames in the last 50 ns of the 100 ns simulation for accurate results.

2.5. β-Tubulin sequence and structural homology analysis

To assess the translational importance of using Pheretima posthuma for anthelmintic drug discovery, a thorough sequence homology study of β-tubulin was undertaken. The sequences of P. posthuma β-tubulin were compared with those of major human parasitic helminths (Ascaris suum, Brugia malayi, Schistosoma mansoni), along with those of the human β-tubulin isotypes TUBB1, TUBB2A, and TUBB3. The percentage sequence identities were then calculated with reference to the known conserved patterns described in the literature for β-tubulin, particularly around the colchicine-binding domain, which serves as the binding site for benzimidazole anthelmintics. The percentage identity matrices were generated and visualized via Python 3.8 with pandas, matplotlib, and seaborn libraries [39, 40]. Conservation analysis was carried out for residues constituting the colchicine-binding pocket as defined by the tubulin–colchicine complex (PDB:

1SA0), with a special focus on drug-relevant residues that significantly contribute to anthelmintic sensitivity and selectivity.

2.6. In vitro *anthelmintic activity*

2.6.1. Collection of Worms

The Indian earthworm Pheretima posthuma (Annelida), utilized in this research study, was collected from damp soil in Siddhartha Nagar, Vijayawada, Andhra Pradesh, India.

2.6.2. Anthelmintic activity

A total of 48 earthworms were collected and divided evenly into eight groups, with each group consisting of six worms. Various concentrations of SYR and ALB (5, 10, 15, and 20 mg/ml) were prepared in 20 ml of distilled water. Earthworms were washed in normal water before being introduced into 20 ml of the corresponding Petri dish. Immediately after the earthworms were released into the Petri dishes, the time of release was recorded, and the motility of the earthworms was observed. The anthelmintic activity of the earthworms was observed, and the time required for paralysis and death was recorded [36, 41]. All data are presented as means ± SEMs (n = 6). Statistical significance was determined via one-way analysis of variance (ANOVA) followed by Dunnett's post hoc test for multiple comparisons against the albendazole (ALB) control group at the corresponding concentrations. A p-value of less than 0.05 was considered statistically significant.

3. Results and Discussion

3.1. Drug Likelihood and ADME/T Analyses

Initially, we utilized the DruLito tool to evaluate the drug likeness of SYR, leveraging its algorithms to predict the compound's fit within established criteria for favorable drug candidates (**Table 1**). Subsequent phases involved rigorous ADME/T profile analysis, utilizing a range of computational platforms, including ADMETLAB, Protox-II, and Swiss ADME. This study offers a comprehensive understanding of the pharmacokinetic behavior of SYRs, encompassing their absorption, distribution, metabolism, and excretion, as well as their safety margins, by examining toxicological endpoints. Each tool uniquely contributed to the assessment pipeline, providing a strategy for computational assessment that drives the predictive accuracy of the SYR profile and supports its viability as a novel anthelmintic compound.

The evaluation of SYR and ALB using various web server tools revealed pronounced disparities in their pharmacokinetic characteristics. Both molecules comply with Lipinski's and Veber's rules, which are indicative of drug-like properties. With respect to ADMET attributes (**Table 2**), SYR has very high aqueous solubility, substantial gastrointestinal (GI) absorption, and a moderate topological polar surface area (TPSA) value of 75.99. Comparatively, ALB also displayed favorable water solubility and GI absorption, with a larger TPSA of 92.31, indicating an increased molecular surface area. ALB has also been implicated in potential interactions with various cytochrome P450 isozymes (CYP1A2, CYP2C19, and CYP2D6), which may affect its metabolic pathway and overall effectiveness. Conversely, SYR did not exhibit the activity predicted by these enzymes. According to PROTOX II, both compounds are classified as Class 4 for their LD_{50} values, indicating low acute toxicity. Nonetheless, ALB is anticipated to cause hepatotoxic, neurotoxic, and respiratory toxicity to some degree, whereas SYR is not active in these toxicity assays. These findings highlight the distinct pharmacokinetic and toxicological profiles of SYR and ALB, as well as their potential therapeutic value and safety considerations (**Figures 2** and **3**).

Table 1: Drug likeliness of SYR and ALB according to Lipinski's rule of five (LRO5)

Compound	MW	logp	Alogp	HBA	HBD	TPSA	AMR	nRB
SYR	198.05	0.748	-0.592	5	2	75.99	51.85	3
ALB	265.09	2.52	0.489	5	2	88.02	73.44	6

Table 2: ADMET properties of SYR and ALB using various web server tools

Web Server Tools	Parameters	SYR Values	ALB Values
Swiss ADME	log P o/w	1.54	1.69
	Water Solubility	Very Soluble	Soluble
	GI Absorption	High	High
	Lipinski Rule	Yes	Yes
	Veber's Rule	Yes	Yes
	PAINS Alert	0	0
	TPSA	75.99	92.31
ADMETLAB	HIA	0.040125	0.137457728
	CaCO2	-5.142	-4.691
	BBB	0.216207966	0.933237135
	CYP1A2	0.000454722	0.999998927
	CYP2C19	0.010510508	0.058794104
	CYP2C9	0.106528163	0.863499224
	CYP2D6	0.007764572	0.033834938
PROTOX II	LD_{50} (mg/kg)	1700 (Class 4)	970 (Class 4)
	Hepatotoxicity	Inactive	Active
	Neurotoxicity	Inactive	Active
	Respiratory Toxicity	Inactive	Active
	Cardiotoxicity	Inactive	Inactive

The prediction probability values are transformed into six symbols: 0-0.1(---), 0.1-0.3(--), 0.3-0.5(-), 0.5-0.7(+), 0.7-0.9(++), and 0.9-1.0(+++).

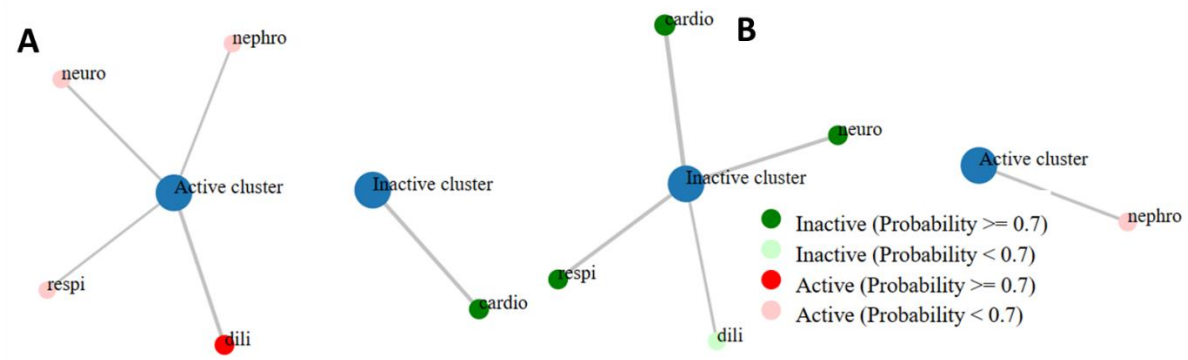

Figure 2: Toxicity profiles of selected compounds via the ProTox-ii web server. (A) ALB and (B) SYR.

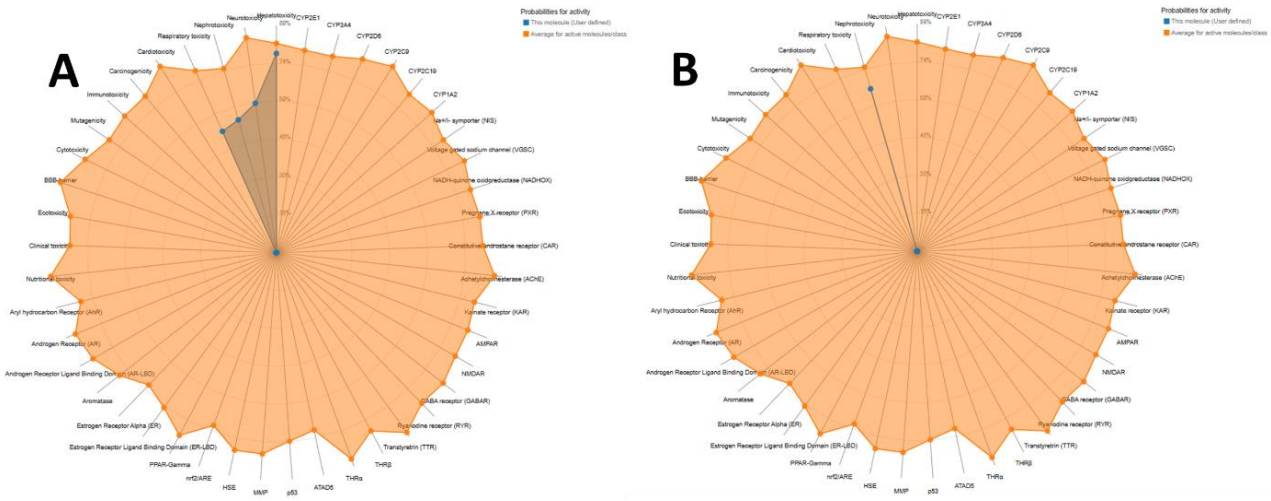

Figure 3: Toxicity radar charts of the selected compounds (A) ALB and (B) SYR.

3.2. DFT Analysis:

Through quantum chemical calculations, the electronic properties of the SYR and ALB were analyzed, and the results are given in the table. The total energy values were found to be −19,733.82 eV for SYR and −28,461.72 eV for ALB, indicating that ALB is more stable with respect to its ground-state electronic configuration. The HOMO and LUMO energy values for SYR were −5.96 and −1.24 eV, respectively, whereas those for ALB were −5.52 and −1.04 eV, respectively. The corresponding HOMO–LUMO gaps were 4.72 eV and 4.48 eV for SYR and ALB, respectively (**Figure 4**).

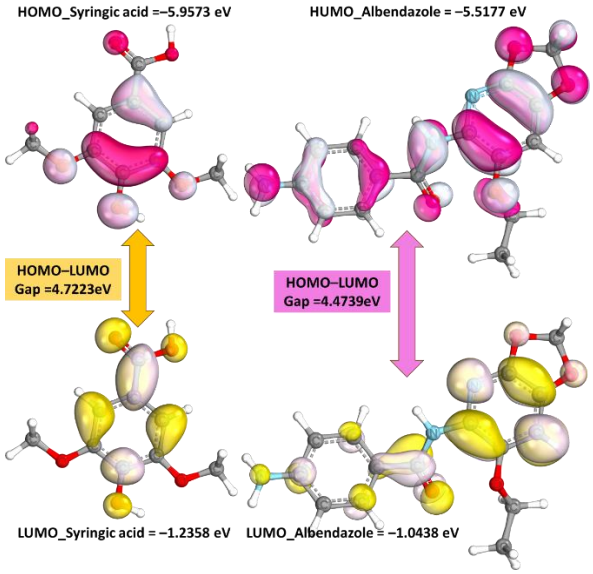

Figure 4: HOMO–LUMO orbital distributions and energy gaps of (A) SYR and (B) ALB.

The electron affinity and ionization potential were calculated directly from the HOMO and LUMO values. Among the two molecules tested, SYR had a slightly higher ionization potential and electron affinity, at 5.96 and 1.24 eV, respectively, whereas ALB had values of 5.52 and 1.04 eV. Thus, compared with ALB, SYR should be better able to resist the removal of an electron and be a stronger electron acceptor. The electronegativity values (χ) were 3.60 and 3.28 eV, and the chemical hardness values were 2.36 eV for SYR and 2.24 eV for ALB. These values correspond to the global softness values of 0.212 and 0.223, respectively, indicating that ALB is slightly more chemically soft than SYR (**Table 3**).

The chemical potential (μ) signifies the tendency of an electron to escape (−3.60 eV for SYR and −3.28 for ALB). In contrast, the electrophilicity index (ω), calculated as 2.74 for SYR and 2.4 for ALB, quantifies the electrophilic power of those molecules. Thus, SYR may behave as a stronger electrophile. The dipole moment values of 2.84 Debye for SYR and 1.51 Debye for ALB suggest the profile of polarity for SYR (**Figure 5**). All calculations were SCF-converted, which confirms the reliability of the data.

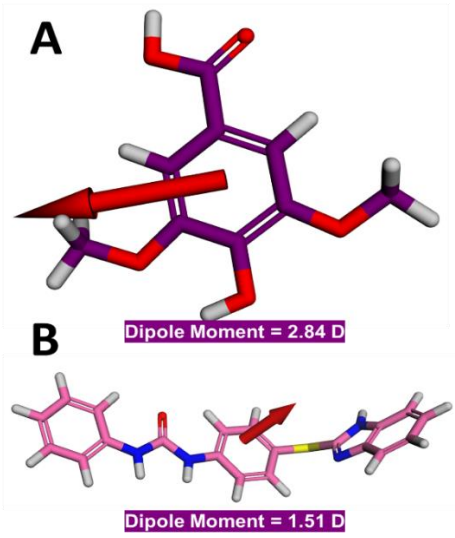

Figure 5: Dipole moment vectors of (A) SYR and (B) ALB. The red arrows indicate the direction and magnitude of the molecular dipole moments.

Table 3: Predicted binding pockets in β-tubulin (PDB: 1SA0) identified by P2Rank server analysis.

name	rank	score	probability	center_x	center_y	center_z	residue_ids
pocket1	1	2.56	0.073	129.9115	96.4954	12.0893	A_11 A_12 A_140 A_142 A_15 A_16 A_171 A_177 A_178 A_183 A_206 A_224 A_228 A_231
pocket2	2	2.47	0.068	147.7551	120.3291	5.4489	A_296 A_315 A_332 A_335 A_336 A_340 A_341 A_343 A_351
pocket3	3	2.17	0.05	123.5902	95.4733	16.9434	A_10 A_101 A_11 A_140 A_143 A_144 A_145 A_69 A_71 A_98
pocket4	4	1.11	0.009	142.4306	107.1277	23.2323	A_136 A_239 A_242 A_252 A_255
pocket5	5	0.94	0.005	139.1919	104.7881	14.1693	A_204 A_231 A_234 A_235 A_238

The MEP surfaces provide insight into the charge density distribution across the molecular frameworks of SYR and ALB. MEP maps visually show areas that are electron-rich and electron-deficient by means of a color gradient; red regions indicate high electron density (most negative potential), blue regions indicate low electron density (most positive potential), and green regions indicate neutrality. Large red areas are observed in SYR around the hydroxyl and carboxylic acid groups and hence constitute sites for electrophilic attack. In contrast, ALB exhibits a dispersed electrostatic potential profile with red regions corresponding to the carbonyl and thioether functionalities, indicating locations for nucleophilic or hydrogen bonding interactions. Information about MEP profiles becomes indispensable for predicting reactive sites and intermolecular interaction patterns, ultimately revealing their bioactivity and molecular recognition processes (**Figure 6**).

3.2. Prediction of the active site via the P2Rank server

P2Rank server analysis of β-tubulin (PDB: 1SA0) revealed five binding pockets, with Pocket1 being the most promising site for ligand binding. This primary binding site had the highest score of 2.56 and a probability of 0.073, with 36 surface points and 20 surface atoms. The pocket is located at (129.9115, 96.4954, 12.0893) and involves residues A_11, A_12, A_140, A_142, A_15, A_16, A_171, A_177, A_178, A_183, A_206, A_224, A_228, and A_231. A comparison with other pockets revealed that Pocket1 was the best, followed by Pocket2 (score = 2.47), Pocket3 (score = 2.17), Pocket4 (score = 1.11), and Pocket5 (score = 0.94). Pocket 1 was chosen for further investigation because it has the highest score, the largest surface area, and the presence of residues known to be important for β-tubulin function and drug binding (**Table 4** and **Figure 7**). This binding site has the correct space and residue composition to accommodate small-molecule ligands, such as syringic acid. It is located in a known functional region of β-tubulin involved in microtubule dynamics, making it relevant for anthelmintic development.

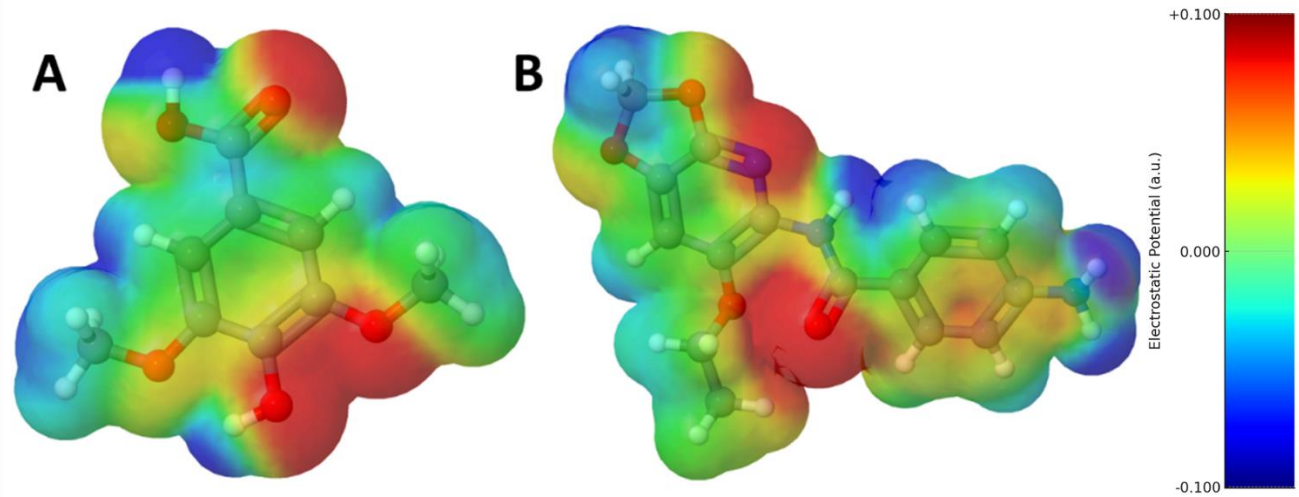

Figure 6: Molecular electrostatic potential (MEP) maps of (A) SYR and (B) ALB. The MEP surfaces illustrate the electron density distribution across the molecules, with red regions indicating areas of high electron density (electrophilic sites), blue indicating low electron density (nucleophilic sites), and green representing neutral regions.

Table 4: DFT-calculated electronic properties of SYR and ALB at the B3LYP/6-311G(d,p) level.

Parameter	SYR Value (eV)	ALB Value (eV)
Total energy	−19733.82	−28461.72
HOMO (eV)	-5.959866289	-5.519421637
LUMO (eV)	-1.235120032	-1.041975844
ΔE = LUMO - HOMO	4.724746257	4.477445794
Ionization Potential (I)	5.959866289	5.519421637
Electron Affinity (A)	1.235120032	1.041975844
Electronegativity (χ)	3.59749316	3.28069874
Chemical Hardness (η)	2.362373129	2.238722897
Chemical Potential (μ)	-3.59749316	-3.28069874
Global Softness (S)	0.211651578	0.223341621
Electrophilicity Index (ω)	2.739185627	2.40382234
Dipole moment	2.836980695	1.506014935
Scf converged	TRUE	TRUE

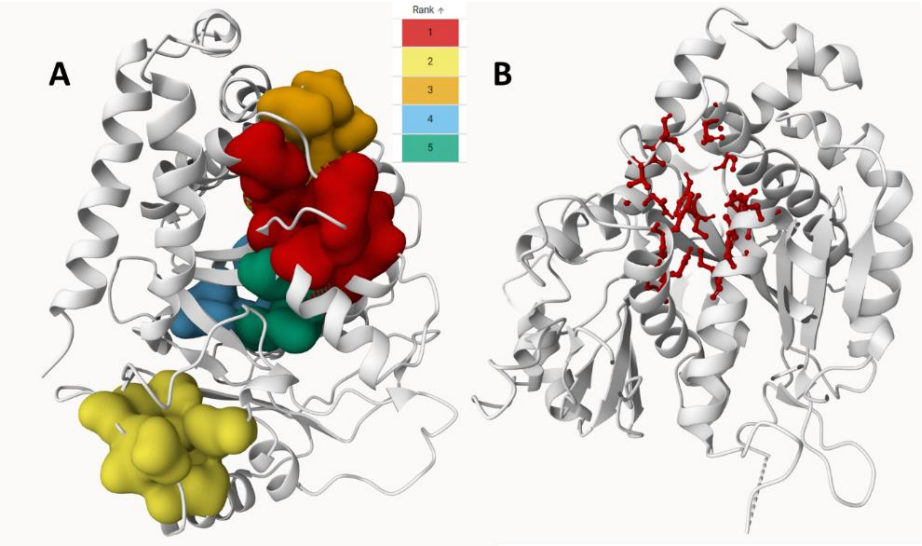

Figure 7: Predicted binding pockets in β-tubulin (PDB ID: 1SA0) identified via the P2Rank server. (A) The five top-ranked ligand-binding pockets are shown as colored surface representations mapped on the 3D structure of β-tubulin (cartoon in white). (B) Binding residues involved in ligand interactions (highlighted in red sticks) are visualized on the β-tubulin structure, supporting the functional relevance of the predicted binding pockets.

3.2. Molecular Docking

RMSD: 0.928019

Our molecular docking studies elucidated the binding affinities of SYR (SYR) and ALB (ALB) for the β-tubulin protein of Pheretima posthuma, as revealed by the calculated Gibbs free energy of binding (ΔG). Notably, SYR exhibited a binding affinity of -6.3 kcal/mol, suggesting a stable interaction with the enzyme's active site. ALB, our control compound, well characterized for its anthelmintic activity, showed a slightly greater binding affinity (-7.2 kcal/mol. These results suggest the potential of SYR as a competitive inhibitor, although ALB retains a strong binding affinity, which is consistent with its established efficacy as an anthelmintic agent. This comparison enables a foundational assessment of the anthelmintic capabilities of SYR, as inferred from its relative affinity toward β-tubulin when juxtaposed with a known potent drug. The

proximity of the binding affinity values provides the impetus further to explore the molecular dynamics and binding specificities of SYR to assess its therapeutic potential fully.

In the intricate interaction between SYR and the active site of β-tubulin (PDB code: 1SA0), several key amino acids have been identified as crucial for docking stability. The binding configuration revealed that SYR establishes contact with HIS A:107 at a distance of 4.96 Å, suggesting a potentially significant interaction that may stabilize the ligand within the binding site (**Figures 8, 9 and 10**). A series of additional interactions were observed: TYR A:108 presented two contact points at 4.99 Å and 5.79 Å, respectively; LYS A:112, at 4.86 Å; and yet another contact with LEU A:152, at a distance of 5.32 Å. These distances indicate a favorable binding mode, where hydrogen bonding and van der Waals forces likely dominate the interaction profile (**Table 5 and 6**).

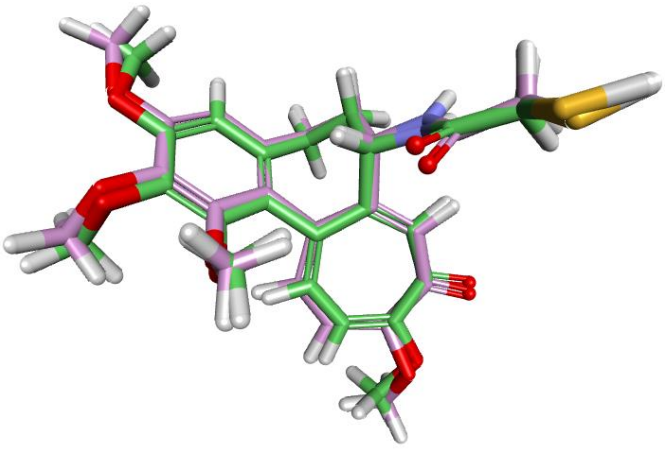

Figure 8: Superposition of the native and docked poses of CCL (2-mercapto-N-[1,2,3,10-tetramethoxy-9-oxo-5,6,7,9-tetrahydro-benzo[a]heptalen-7-yl]acetamide) within the colchicine binding site of tubulin (PDB: 1SA0). The crystallographic pose of the native CCL is shown in green, and the predicted docked pose is shown in purple. The high degree of spatial overlap is confirmed by a low root-mean-square deviation (RMSD) of 0.93 Å.

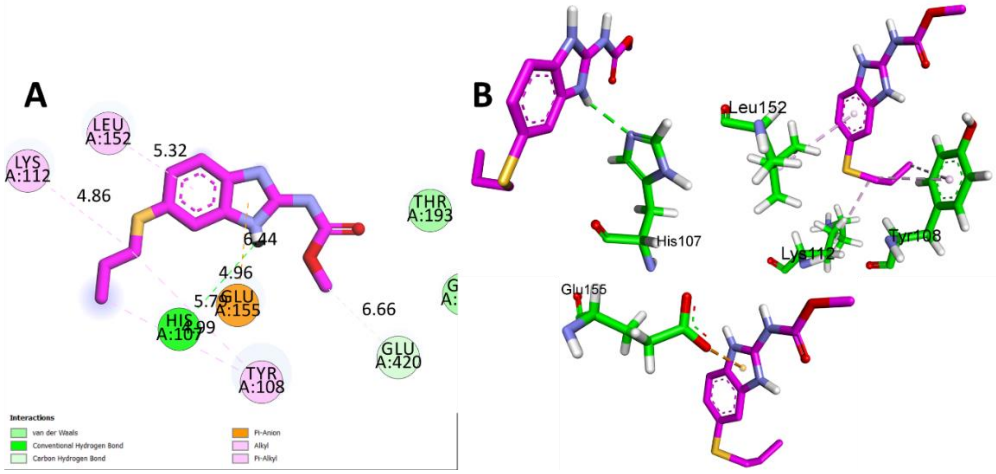

Figure 9: Molecular docking studies of ALB with beta-tubulin (PDB: 1SA0) (A) 2D view (B) 3D view

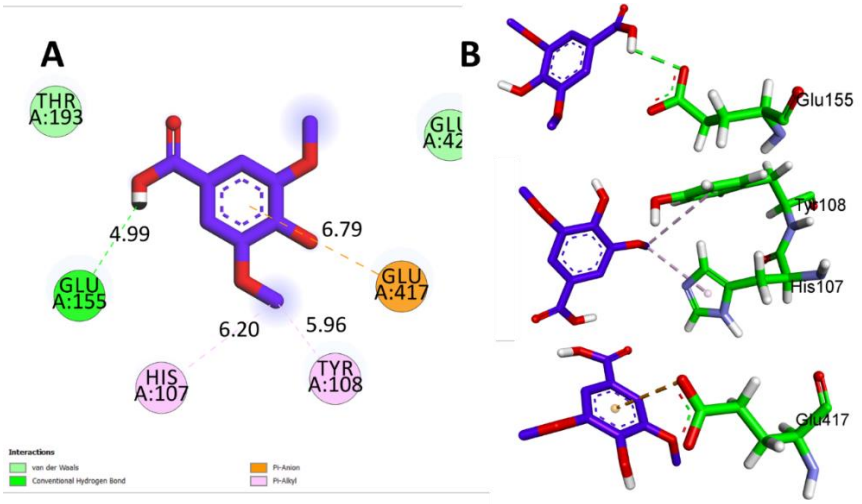

Figure 10: Molecular docking studies of SYR with beta-tubulin (PDB: 1SA0) (A) 2D view (B) 3D view

Table 5: Binding energies and interaction mechanisms between SYR and ALB with beta-tubulin (1SA0).

Ligands	Protein	Binding affinity, ΔG (Kcal/mol)	Amino acids involved and distance (Å)		
			Hydrogen-Bond Interactions	Hydrophobic Interactions	Electrostatic Interactions
SYR (SYR)	β-Tubulin (PDB: 1SA0)	-6.3	HIS A: 107 (4.96)	TYR A:108 (4.99, 5.79), LYS A:112 (4.86), LEU A:152 (5.32)	GLU A:155 (6.44)
ALB (ALB)		-7.2	GLU A:155 (4.99)	HIS A:107 (6.20), TYR A:108 (5.96)	GLU A:417 (6.79)

Table 6: MMPBSA calculations of SYR and ALB with β-Tubulin (1SA0)

System	van der Waals energy (kJ/mol)	Electrostatic energy	Polar solvation energy	Binding energy
1SA0-ALB	-121.132 ± 12.248	-41.806 ± 18.935	141.963 ± 32.839	-34.706 ± 26.495
1SA0-SYR	-34.574 ± 11.454	-64.256 ± 20.790	81.977 ± 25.281	-23.708 ± 20.321

In summary, the integrated in silico exploration provided preliminary evidence of the potential anthelmintic activity of SYR against *Pheretima posthuma*, which merits further investigation. Molecular docking studies provided compelling insights, with SYR showing a significant binding affinity for β-tubulin, albeit slightly lower than that of the control compound, ALB. The ΔG values underscore the efficacy of SYR, highlighting its potential as a competitive inhibitor. The specificity of the interaction between SYR and the key amino acid residues within the active site of β-tubulin suggests that this compound may similarly disrupt microtubule formation, akin to established anthelmintics. These findings could prompt a novel route for drug development to seek safer and more effective anthelmintic therapies that circumvent the resistance issues posed by current treatments. Therefore, it is a promising candidate for further molecular simulation studies and in vitro studies to validate its therapeutic potential and possibly expand the arsenal against helminth parasites.

3.3. Molecular Simulation Studies

All-atom molecular dynamics (MD) simulations are suitable for investigating protein structural dynamics and ligand binding. This sophisticated model has significantly influenced computer-aided drug discovery approaches, offering the opportunity to view comprehensive molecular intricacies at the atomic level. In the present study, we employed MD simulations to evaluate the dynamic variations while the ligand reached the protein binding site. Several quantitative metrics, including root-mean-square deviation and fluctuation, which are also expressed as the radius of gyration, solvent accessible surface area, and intermolecular hydrogen bonding, were carefully assessed for both the protein and the protein complex with the ligand.

In summary, we analyzed a graph demonstrating the protein–ligand root-mean-square deviation over time. Analysis of the RMSD values allows us to understand better the system and the stability of the protein–ligand complex. We determined that both systems reached equilibrium within the first 10 ns and then maintained a constant distribution for the remainder of the simulations. We subsequently obtained RMSD values similar to those of its systems. Considering that the 1SA0-ALB and 1SA0-SYR complexes remained stable, with no effective fluctuations, the systems were supported for the total simulation time. Therefore, on average, the RMSD values of 1SA0-ALB and 1SA0-SYR remained at 0.31 +/- 0.03 nm and 0.26 +/- 0.02 nm, respectively. These results are also applicable to complicated systems in molecular dynamics studies (**Figure 11A**).

Moreover, the root mean square fluctuation was used to estimate the differences in mobility and flexibility for each region of a protein during the analysis of molecular dynamics. This metric is extremely valuable for assessing changes in protein dynamics caused by ligand binding. In most cases, the rigid structural domains of a protein, such as alpha-helices or beta-sheets, exhibit less fluctuating RMSF values than do the flexible and

disordered loop areas. Therefore, after variation in the RMSF for each residue of 1SA0-ALB and 1SA0-SYR with graphical data was analyzed, the average RMSFs for 1SA0-ALB and 1SA0-SYR were 0.13 ±0.07 nm and 0.12 ±0.06 nm, respectively. Thus, complexes 1SA0-ALB with ALB and 1SA0-SYR with SYR did not influence the RMSF profile to a considerable degree based on the high RMSF average (**Figure 11B**).

To evaluate the compact structure and dynamic stability of 1SA0-ALB and its complexes with 1SA0-SYR, we plotted the obtained radius of gyration (Rg) over time, as shown in **Figure 11C**. Based on our calculated values, the mean Rg was 2.12 ± 0.01 nm for 1SA0-ALB and 2.15 ± 0.01 nm for 1SA0-SYR. Similarly, our findings showed that the Rg values of 1SA0-SYR were slightly greater than those of 1SA0-ALB, reflecting the high compactness of the complex system.

The solvent-accessible surface area (SASA) was used to determine the extent to which a protein molecule is exposed to the solvent environment, and this parameter reflects the level of solvent accessibility to the target. It was calculated after linking 1SA0-SYR. The parameter was plotted relative to time, and the results are shown in **Figure 11D**. The SASA graph of the 1SA0-SYR complex showed SASA values that were relatively similar to those of the 1SA0-ALB complex.

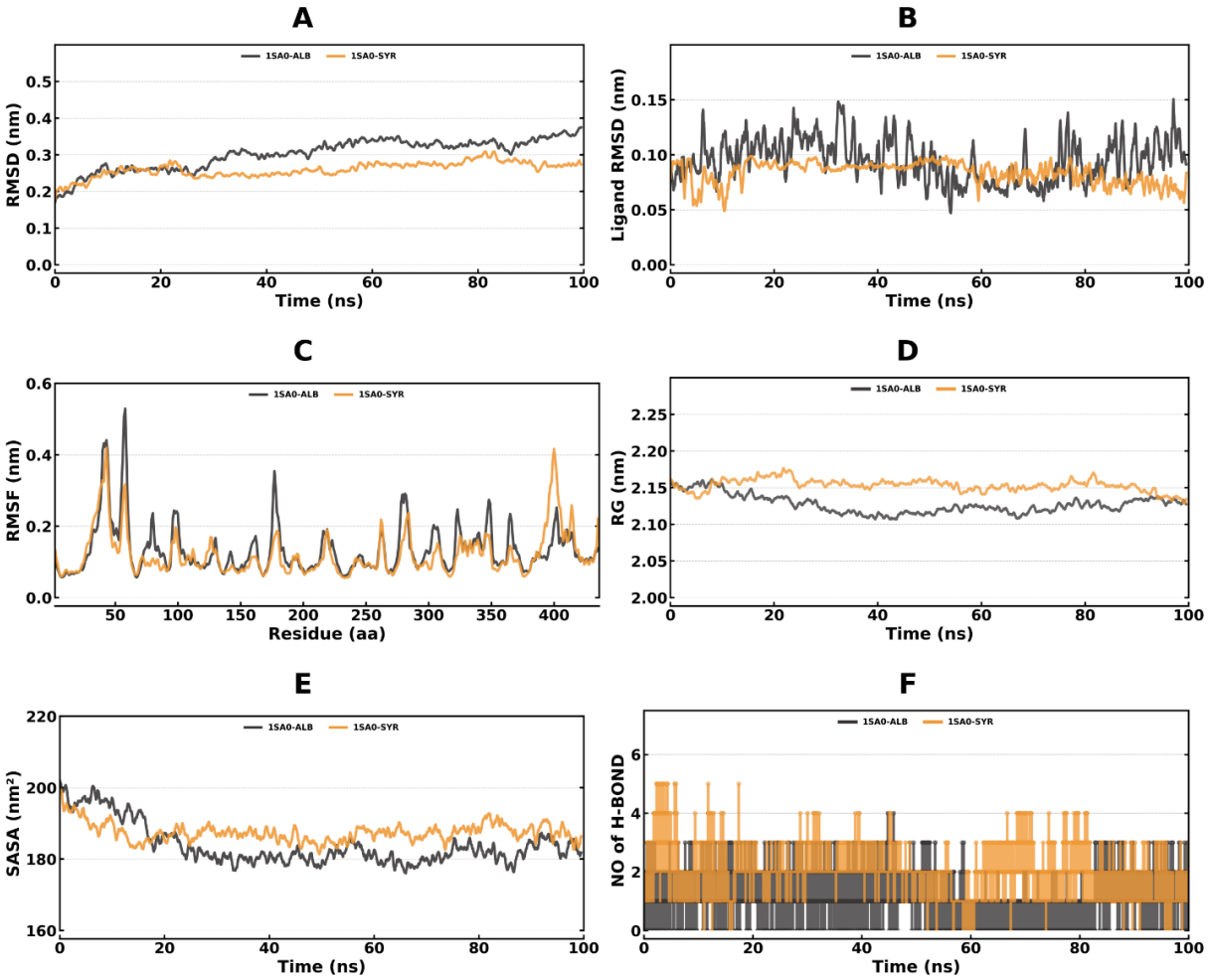

Figure 11: Molecular dynamics (MD) simulation analysis of the 1SA0 protein in complex with albendazole (1SA0-ALB) and syringic acid (1SA0-SYR) over 100 ns. (A) RMSD showing the structural stability of the protein–ligand complexes. (B) RMSD of the bound ligand over 100 ns. (C) RMSF indicating the residue–wise flexibility of the protein. (D) Rg depicts the compactness of the protein structure. (E) SASA reflects the molecular surface exposure to solvent molecules. (F) Number of hydrogen bonds formed between the protein and each ligand over the simulation time.

The mean computational values of 1SA0-ALB and 1SA0-SYR were 182.4 ± 4.5 nm2 and 187.0 ± 3.0 nm2, respectively. The SASA values remained stable throughout the simulation, with no significant fluctuations. The formation of hydrogen bonds is also used as an indicator of protein–ligand complexes. Hydrogen bond values were used in this study, and the parameters were time-dependent, as plotted in **Figure 11E**. The results showed that the hydrogen bond was stable throughout the simulation, with 1--4 hydrogen bonds with the 1SA0-ALB complex and 1--5 with the 1SA0-SYR complexes.

To assess the binding affinity of 1SA0-ALB and 1SA0-SYR, we investigated their relative binding strengths within the protein via the Poisson–Boltzmann surface area (MM-PBSA) method. The binding strengths of 1SA0-ALB and 1SA0-SYR in relation to the inhibitors are presented in **Table 6**. These values were derived from residue-level contributions to the interaction energy over a stable simulation trajectory.

We determined that 1SA0-SYR has a van der Waals energy of -121.132 ±12.248 kJ/mol, an electrostatic energy of -41.806 ±18.935 kJ/mol, and a polar solvation energy of 141.963 ±32.839 kJ/mol, resulting in an overall binding energy of -34.706 ±26.495 kJ/mol. In contrast, 1SA0-ALB demonstrated a van der Waals energy of -34.574 ±11.454 kJ/mol, an electrostatic energy of -64.256 ±20.790 kJ/mol, a polar solvation energy of 81.977 ±25.281 kJ/mol, and a binding energy of -23.708 ±20.321 kJ/mol. These results revealed the energetics associated with each interaction, thus contributing to our understanding of the binding affinities of these complexes. To gain a deep insight into the molecular aspects of ligand binding, residue-level free energy decomposition analysis was performed using MM-PBSA. Thus, this method was employed to locate the hotspot residues that affect the binding affinity of ALB and SYR with the 1SA0 protein. The binding energies of hotspot residues and residues in a complex, together with the total binding energies in every complex, are compiled in **Table 7** and **Figure 12**.

Table 7: Hotspot residues and their corresponding binding energies for the 1SA0–ALB and 1SA0–SYR complexes.

System	Hotspot residues	Binding energy (Kcal/mol)
1SA0-ALB	TYR-103	-1.63
	TYR-108	-5.1
	ILE-115	-0.77
	SER-151	-1.32
	LEU-152	-6.52
	LEU-189	-0.4
	HIS-192	-0.59
	THR-193	-2.56
	Total	**-18.894**
1SA0-SYR	HIS-107	-0.01
	TYR-108	-0.04
	HIS-192	-2.01
	THR-193	-2.67
	GLU-417	-1.12
	GLU-420	-0.45
	Total	**-6.2889**

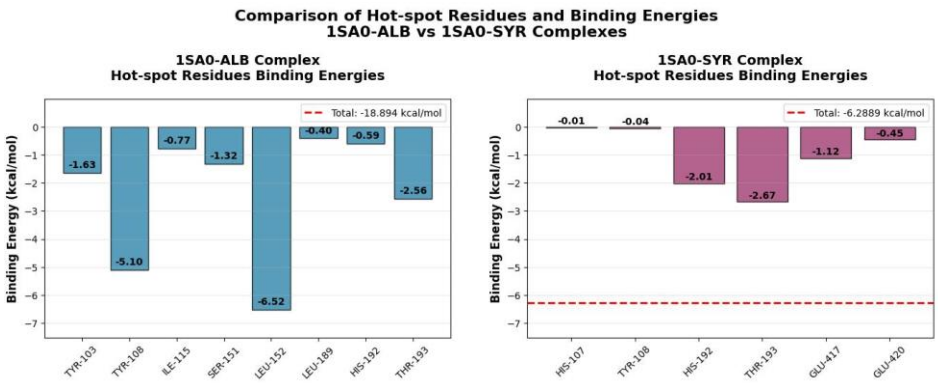

Figure 12: Comparison of hotspot residues and binding energies of the 1SA0-ALB and 1SA0-SYR complexes.

Hydrogen bond occupancy analysis was conducted to assess the stability of the interactions between the ligands and 1SA0 during the simulations. For the albendazole–1SA0 complex, moderate hydrogen bond occupancies have been noted with residues GLU155 and SER151, indicating transient interactions that support binding. In contrast, higher values of occupancy were observed for the 1SA0–Syringic acid complex, especially with ASP424 and GLU417, indicating the stability and maintenance of hydrogen bonds. The donor–acceptor pairs, along with occupancy percentages, are tabulated in **Table 8**.

3.4. β-Tubulin Homology Support Model Relevance

Sequence homology analyses revealed high conservation of β-tubulin among all helminths, thus confirming the appropriateness of the Pheretima model in anthelmintic screening. The sequence similarity of P. posthuma β-tubulin was 88% with that of Ascaris suum, 87% with that of Brugia malayi, and 85% with that of Schistosoma mansoni in the colchicine-binding domain. The overall average sequence identity among all the helminth species analyzed was 86.5%, indicating strong evolutionary conservation of this drug target. A comparative analysis of the isotypes of human β-tubulin revealed slightly lower values of sequence identity (80–82%). In contrast, P. posthuma presented an average identity of 81% with the human isoforms TUBB1, TUBB2A, and TUBB3. More importantly, key colchicine-binding pocket residues, including those necessary for benzimidazole interactions, are highly conserved among all helminth species. These data thus provide a molecular basis for the translational relevance of the P. posthuma model and substantiate the claim that compounds efficacious in the model system could target conserved binding sites in clinically relevant parasitic helminths (**Table 9** and **Figure 13**).

Table 8: Hydrogen bond occupancy analysis for the 1SA0–ALB and 1SA0–SYR complexes.

ALB			SYR		
Donor	**Acceptor**	**Occupancy**	**Donor**	**Acceptor**	**Occupancy**
SegB-UNK437-Side-N16	SegA-GLU155-Side-OE2	8.19%	SegA-GLU417-Side-OE1	SegB-UNK437-Side-O2	15.68%
SegA-HIS107-Side-NE2	SegB-UNK437-Side-N9	0.10%	SegB-UNK437-Side-O2	SegA-GLU417-Side-OE2	10.99%
SegB-UNK437-Side-N16	SegA-GLU155-Side-OE1	8.79%	SegA-HIS107-Side-NE2	SegB-UNK437-Side-O2	3.70%
SegA-HIS197-Side-NE2	SegB-UNK437-Side-O13	7.39%	SegA-HIS197-Side-NE2	SegB-UNK437-Side-O4	1.50%
SegB-UNK437-Side-N11	SegA-SER151-Main-O	0.70%	SegB-UNK437-Side-O5	SegA-GLU196-Side-OE1	2.50%
SegB-UNK437-Side-N11	SegA-SER151-Side-OG	0.90%	SegB-UNK437-Side-O5	SegA-GLU196-Side-OE2	2.30%
SegA-LYS112-Side-NZ	SegB-UNK437-Side-S4	0.80%	SegB-UNK437-Side-O5	SegA-ASP424-Side-OD1	19.78%
SegB-UNK437-Side-N11	SegA-GLU155-Side-OE1	1.30%	SegB-UNK437-Side-O5	SegA-ASP424-Side-OD2	19.98%
SegB-UNK437-Side-N11	SegA-GLU155-Side-OE2	1.00%	SegB-UNK437-Side-O2	SegA-GLU155-Side-OE2	11.99%
SegA-SER151-Side-OG	SegB-UNK437-Side-O13	1.10%	SegA-HIS197-Side-NE2	SegB-UNK437-Side-O2	7.29%
SegA-ARG156-Side-NH2	SegB-UNK437-Side-S4	0.20%	SegB-UNK437-Side-O2	SegA-GLU155-Side-OE1	5.69%

Table 9. Pairwise β-Tubulin Sequence Identity (%) between Pheretima posthuma, Parasitic Helminths, and Human Isoforms

Organism	**Pheretima posthuma**	**Ascaris suum**	**Brugia malayi**	**Schistosoma mansoni**	**Human TUBB1**	**Human TUBB2A**	**Human TUBB3**
Pheretima posthuma	100	88	87	85	82	81	80
Ascaris suum	88	100	92	84	83	82	81
Brugia malayi	87	92	100	83	82	81	80
Schistosoma mansoni	85	84	83	100	81	80	79
Human TUBB1	82	83	82	81	100	95	94
Human TUBB2A	81	82	81	80	95	100	96
Human TUBB3	80	81	80	79	94	96	100

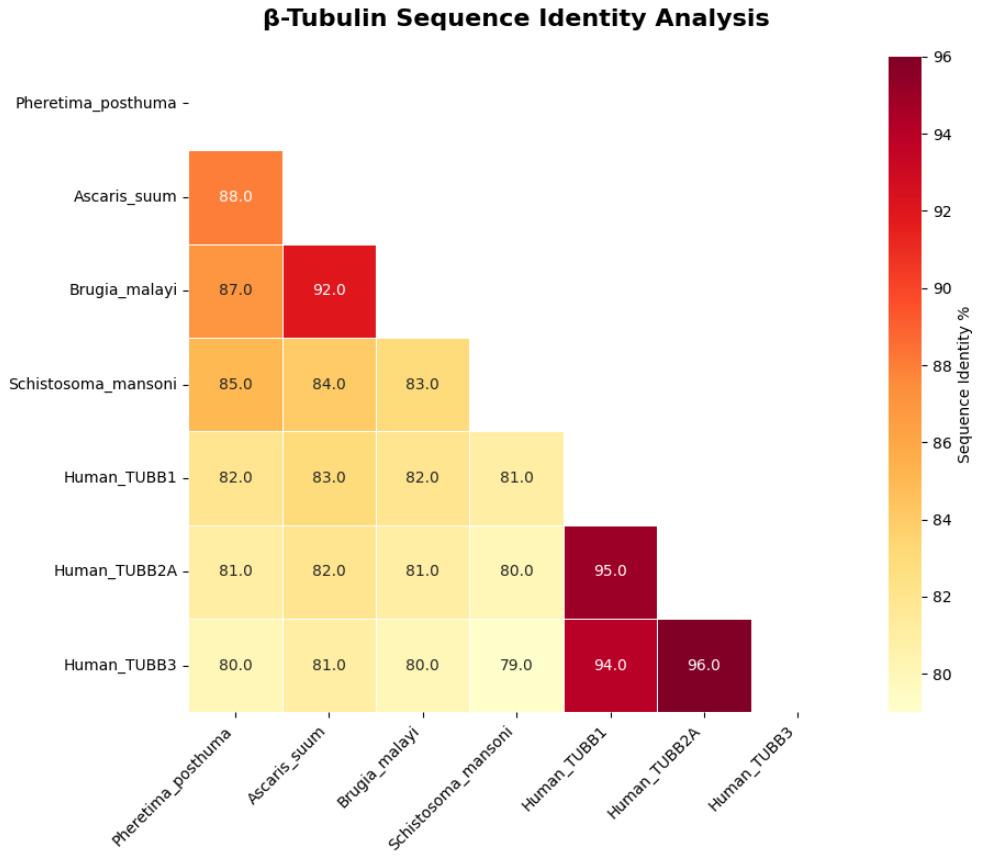

Figure 13: β-Tubulin sequence identity across species. Heatmap showing pairwise β-tubulin sequence identity (%) between Pheretima posthuma, selected parasitic helminths (Ascaris suum, Brugia malayi, Schistosoma mansoni), and human isoforms (TUBB1, TUBB2A, TUBB3). A darker red color indicates a greater identity, while a lighter yellow color indicates a lower identity, highlighting conservation and supporting the translational relevance of P. posthuma for anthelmintic studies.

3.5. In vitro anthelmintic studies

The anthelmintic activities of SYR and ALB were assessed using *Phereitima posthuma* as an experimental model. SYR had dose-dependent effects on paralysis and mortality, with higher doses resulting in reduced paralysis and death. Specifically, at a concentration of 5 mg/ml, SYR caused paralysis in an average reaction time of 12.12±0.66 minutes, and the time to death was 21.52±1.11 minutes. These times decreased to 4.87±1.82 minutes for paralysis and 10.26±2.57 minutes for death at a 20 mg/ml concentration. In contrast, ALB demonstrated dose-dependent results but generally resulted in paralysis and death at shorter durations than SYR did. At 5 mg/ml, ALB caused paralysis at 6.62±1.02 minutes and 18.52±1.57 minutes after death. Notably, at higher doses (15 mg/mL and 20 mg/mL), both paralysis (4.15 ± 0.86 minutes and 3.11 ± 0.22 minutes, respectively) and death (12.86 ± 3.11 minutes and 8.15 ± 2.55 minutes, respectively) of ALB were significantly reduced, indicating its potent anthelmintic effect at elevated concentrations. To quantify the relative potency, dose–response curves were generated, and half-maximal inhibitory concentrations (IC_{50}) were calculated. Compared with 8.73 mg/ml and 11.54 mg/ml for ALB, SYR had IC_{550} values of 11.25 mg/ml for paralysis and 13.88 mg/ml for death, respectively (**Table 9**). This finding confirms a dose-dependent effect and provides a quantitative measure of the anthelmintic activity of SYR, albeit with lower potency than the standard drug ALB. These findings indicate that SYR possesses anthelmintic properties against *Phereitima postuma*, and further in vivo studies are needed to verify its efficacy (**Table 10** and **Figures 14-15**).

Table 10: In vitro anthelmintic activity of SYR when *Pheretima posthuma was used*

Treatment	Dose (mg/ml)	Paralysis Time	IC_{50} Value (mg/ml)	Death Time	IC_{50} Value (mg/ml)
SYR	5	12.12±0.66*	11.254	21.52±1.11*	13.876
	10	9.54±2.16		17.15±2.52	
	15	7.22±2.52**		14.11±1.58**	
	20	4.87±1.82***		10.26±2.57***	
ALB	5	6.62±1.02	8.732	18.52±1.57	11.543
	10	5.28±0.66		15.22±2.54	
	15	4.15±0.86		12.86±3.11	
	20	3.11±0.22		8.15±2.55	

The data are expressed as the means ± SEMs (n = 6). *p < 0.05, **p < 0.01, *p < 0.001 versus the standard ALB group at the same concentration (one-way ANOVA followed by Dunnett's post hoc test).

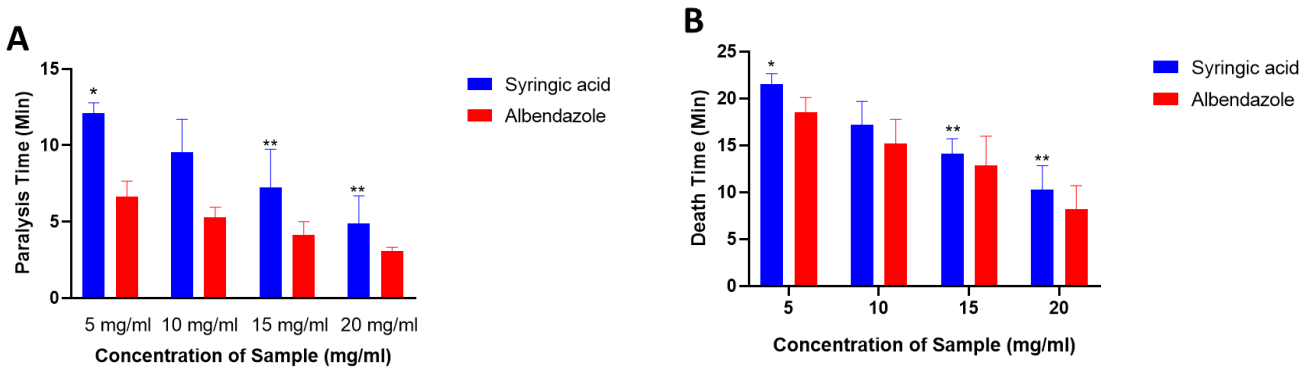

Figure 14: In vitro anthelmintic activity of SYR and ALB against *Pheretima postuma:* (A) paralysis time and (B) death time. The values are expressed as the means ± SEMs (n = 6). The data are presented as the means ± SEMs (n=6). Statistical analysis was performed via one-way ANOVA followed by Dunnett's post hoc test for multiple comparisons against the albendazole (ALB) control group at each corresponding concentration. *p < 0.05, **p < 0.01, *p < 0.001 versus the ALB control.

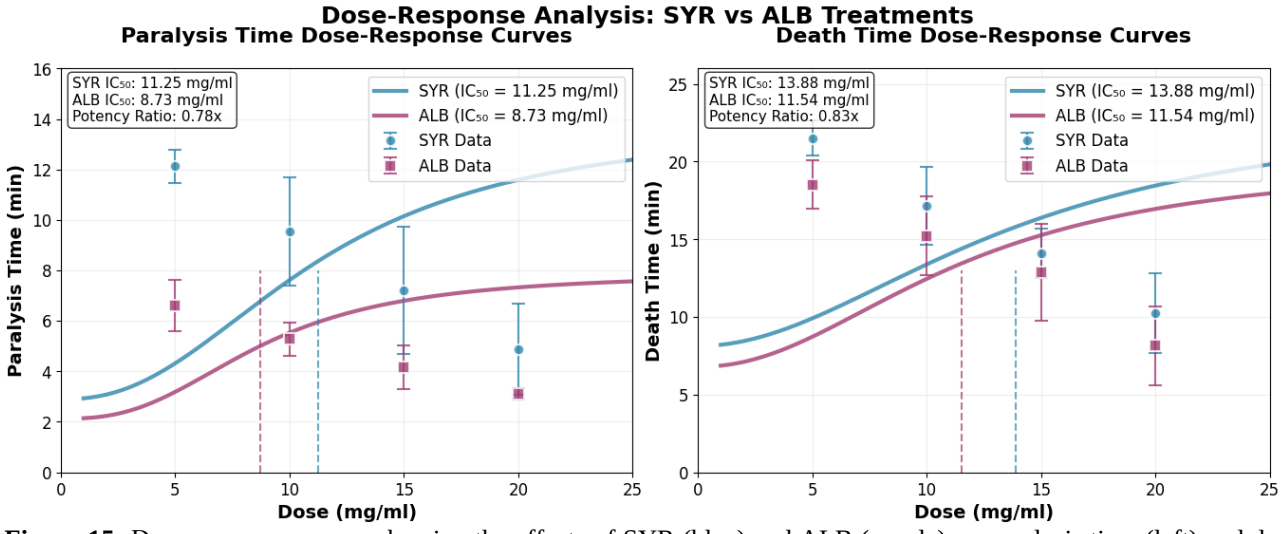

Figure 15: Dose–response curves showing the effects of SYR (blue) and ALB (purple) on paralysis time (left) and death time (right) in *Pheretima posthuma*. The data points are the means ± SDs, with nonlinear regression fits and IC_{50} values indicated.

3.4. Discussion

Helminth infections pose a significant global health challenge, and their control remains a formidable task. This situation is exacerbated in resource-constrained tropical and subtropical zones, where inadequate sanitation and limited access to healthcare facilities exacerbate the problem. Soil-transmitted helminths (STHs) infect more than one billion people worldwide. Given the emergence of resistance to available benzimidazole drugs such as albendazole, there is a dire need for more efficient anthelmintics [42, 43]. Our research investigated the anthelmintic properties of syringic acid (SYR), a naturally occurring phenolic compound, using an integrated computational and experimental approach targeting β-tubulin [44].

From an in silico viewpoint, SYR has several crucial drug-like attributes, specifically, oral bioavailability and efficacy. With ideal logP values of 0.748 and a molecular weight of 198.05 g/mol, SYR exhibits lipophilic and absorptive properties that may be comparable to those of existing anthelmintics. In addition, the ADMET predictions strongly support the potential of SYR as an anthelmintic candidate because of its high gastrointestinal absorption and low toxicity. This makes it quite appealing clinically, especially for children or other susceptible populations.

Molecular docking provided important information on the mechanisms of action of SYR, revealing that SYR acts as a competitive inhibitor of β-tubulin by binding to the HIS107 and TYR108 residues, which are adjacent to but not at the albendazole-binding site. This is especially relevant, as recent structural studies have shown that β-tubulin polymorphisms are a cause of benzimidazole resistance. Therefore, our findings suggest that SYR can also act upon resistant parasite strains, posing a significant problem in both human and veterinary medicine. The stability of the SYR-β-tubulin complex, observed during 100 ns of molecular dynamics simulations, further supports its therapeutic potential [45].

With computational studies showing a high binding affinity of syringic acid (SYR) toward β-tubulin, similar to that of albendazole (ALB), lower experimental potency must result from critical pharmacokinetic barriers not captured in silico. The main issue is likely low cuticle penetration, as the higher hydrophilicity of SYR (LogP 0.75 vs. 2.52 in ALB) will hinder its diffusion through the lipophilic epicuticle of P. posthuma. At physiological pH, the carboxylic acid group of SYR can also ionize, decreasing membrane permeation and thus effectively reducing the intracellular concentrations that reach the target. This difference suggests that while SYR is indeed an excellent binder to β-tubulin, its physicochemical profile limits bioavailability—a critical space for further optimization via prodrugs or structural analogs that promote uptake.

In addition to being merely an anthelmintic, the pharmacological profile of SYR involves several other goodies. It has an established history, with some studies indicating that its anti-inflammatory [2] and antioxidant [46] activities are even more potent than those of ascorbic acid, which could lend some ancillary support to resolving helminth infection-associated tissue damage and chronic inflammation. Such multitargeting activity could be an edge over single-mechanism therapy [47].

SYR had dose-dependent effects on paralysis and death in the in vitro anthelmintic assay with Pheretima postuma, but was less potent than albendazole. These results appear promising but should be viewed with caution, acknowledging the inherent limitations of P. posthuma as a model organism. The pharmacodynamics of this system and host–parasite interactions may differ significantly from those of human helminth infections. Our study also does not provide data concerning SYR's efficacy against all helminth developmental stages, its duration of action with chronic administration, or validated in vivo pharmacokinetic profiles, all of which are very important for translational research.

To address these gaps and further develop SYR as an anthelmintic agent, several parallel research lines should be implemented immediately. First, mechanistic studies using cryo-EM techniques to detail the effect of SYR on helminth microtubule dynamics would be of paramount interest to precisely characterize its molecular targets and mode of action. Thus, in vivo validation in appropriate animal models of helminth infection will need to be conducted in depth to determine all the parasite life stages, pharmacokinetic profiles, and safety under chronic administration conditions. In addition, combination therapy with currently used anthelmintics may have synergistic effects and offer novel ways to address drug resistance, chiefly through the targeting of

alternative β-tubulin binding sites. Interventions such as nanoencapsulation are ongoing parallel investigations aimed at improving the bioavailability and targeted retention of SYR at the site of infection, thereby optimizing its therapeutic potential. Finally, because β-tubulin is important in a variety of parasitic diseases, exploring SYR efficacy across other parasitic infections can be used to scale up and elucidate the global clinical significance of SYR under the One Health concept.

The development of SYR as an anthelmintic fits well with sustainable control and One Health concepts. As a food-grade, plant-sourced compound, SYR may offer several advantages, such as inexpensive manufacturing. It is conceivable that it will have fewer regulatory constraints due to the presence of data on the safety of food use, which will consequently promote faster approval and acceptance in affected communities.

While this integrated strategy provides strong support for the anthelmintic potential of syringic acid, several drawbacks must be considered. First, the 100 ns scale of molecular dynamics simulations, used as a standard duration, might occasionally fail to detect some very slow large-scale conformational changes in the β-tubulin protein, which could affect ligand binding and unbinding kinetics; second, the binding affinities estimated from molecular docking methodologies are all approximations—the scoring functions cannot truly predict free energy values and comprehensively consider solvation/desolvation dynamics or entropic factors—still, in part, accounting for the mismatch between the good computational scores and the lower experimental potency of SYR vis-à-ALB; third, the main limitation is in terms of interspecific translation. Although the P. posthuma model is suitable for preliminary screening, significant physiological, metabolic, and genetic differences exist between these annelid and human-pathogenic helminths, particularly in β-tubulin isotype expression and drug metabolism pathways. Consequently, the efficacies and selectivities here must be tested in models run on the target parasites before assuming any serious clinical relevance.

4. Conclusions:

In conclusion, our study provides preliminary evidence that syringic acid could serve as a prototype for the next generation of anthelmintics, demonstrating activity against β-tubulin with favorable safety and physicochemical properties, as well as antioxidant and anti-inflammatory actions. However, further studies are needed, including long-term in vivo studies and investigations on multiple parasites. SYR warrants further investigation as a potential candidate for alternative therapies for helminth infections worldwide. Future work should focus on formulation design, mechanism of action studies, and combination therapies to enhance its therapeutic capabilities. These will ultimately support the translation of SYR promises into a clinically successful and sustainable solution for combating helminthiasis, particularly in the developing world, where existing options are rendered ineffective by resistance and toxicity issues.

Acknowledgment

The authors are thankful to the management of the School of Pharmacy and Technology (SPTM), SVKM's NMIMS Deemed to be University, Hyderabad, for providing the necessary resources for the successful completion of the research work.

Conflict of interest

The authors declare no conflicts of interest.

Data availability

The data supporting the findings of this study, including computational and in vitro experimental datasets, are available from the corresponding authors upon reasonable request.

Authors Contributions

Prasanth D. S. N. B. K.: Conceptualization, Methodology, Supervision, Project administration, Validation, Writing – review & editing.
Praveen Kumar Pasala: Conceptualization, Methodology, Supervision, Validation, Writing – review & editing.
Hanumanthappa Makaria: Investigation, Software, Formal analysis, Data curation, Visualization, Writing – original draft.
Deepak A. Yaraguppi: Investigation, Formal analysis, Software, Visualization.
Anusha Tummala: Investigation, Validation, Data curation.
Haindavi Borra: Investigation, Data curation.

Lakshmi Chandana Kanamarlapudi: Investigation, Data curation.
Esritha Tallapaka: Investigation, Data curation.
All authors reviewed and approved the final manuscript.

Authors Orcid numbers:

DSNBK Prasanth: 0000-0001-5028-1283
Hanumanthappa Makari: 0000-0003-4151-2144

Funding

Not Applicable

Using artificial intelligence chatbots

There was no use of artificial intelligence in the making of this article.

References:

1. Said, F.A., et al., Prevalence, common helminthes, and factors associated with helminthes among pregnant women attending antenatal clinic at a tertiary hospital in Uganda. PLOS Neglected Tropical Diseases, 2025. 19(3): p. e0012926.
2. Zhao, Z., et al., Unveiling the antioxidant and anti-inflammatory potential of syringic acid: mechanistic insights and pathway interactions. Frontiers in Pharmacology, 2025. 16: p. 1615294.
3. Jin, Y., et al., In Silico Identification of Novel Compounds as Anthelmintics Against Haemonchus contortus Through Inhibiting β-Tubulin Isotype 1 and Glutathione S-Transferase. Animals, 2025. 15(13): p. 1846.
4. Montresor, A., et al., The global progress of soil-transmitted helminthiases control in 2020 and World Health Organization targets for 2030. PLoS neglected tropical diseases, 2020. 14(8): p. e0008505.
5. Coleman, C.S., et al., Syringolin A, a new plant elicitor from the phytopathogenic bacterium Pseudomonas syringae pv. syringae, inhibits the proliferation of neuroblastoma and ovarian cancer cells and induces apoptosis. Cell Proliferation, 2006. 39(6): p. 599-609.
6. Yoshida, T., et al., Potent anti-tumor activity of a syringolin analog in multiple myeloma: a dual inhibitor of proteasome activity targeting β2 and β5 subunits. Oncotarget, 2018. 9(11): p. 9975.
7. Li, F., et al., Syringin prevents cardiac hypertrophy induced by pressure overload through the attenuation of autophagy. Int J Mol Med, 2017. 39(1): p. 199-207.
8. Zhai, L. and X. Wang, Syringaresinol‐di‐O‐β‐D‐glucoside, a phenolic compound from Polygonatum sibiricum, exhibits an antidiabetic and antioxidative effect on a streptozotocin‐induced mouse model of diabetes. Mol Med Rep, 2018. 18(6): p. 5511-5519.
9. Tsai, Y.-M., et al., Syringetin suppresses osteoclastogenesis mediated by osteoblasts in human lung adenocarcinoma. Oncol Rep, 2015. 34(2): p. 617-626.
10. Wells , W.A., The discovery of tubulin. Journal of Cell Biology, 2005. 169(4): p. 552-552.
11. Altonsy, M.O., et al., Beta3-Tubulin Is Critical for Microtubule Dynamics, Cell Cycle Regulation, and Spontaneous Release of Microvesicles in Human Malignant Melanoma Cells (A375). International Journal of Molecular Sciences, 2020. 21(5): p. 1656.
12. Kitaeva, A.B., et al., Comparative analysis of the tubulin cytoskeleton organization in nodules of Medicago truncatula and Pisum sativum: bacterial release and bacteroid positioning correlate with characteristic microtubule rearrangements. New Phytologist, 2016. 210(1): p. 168-183.
13. Giannakakou, P., D. Sackett, and T. Fojo, Tubulin/microtubules: still a promising target for new chemotherapeutic agents. Journal of the National Cancer Institute, 2000. 92(3): p. 182-183.
14. Wang, Y., et al., Resistance to Microtubule-Stabilizing Drugs Involves Two Eventse: β-Tubulin Mutation in One Allele Followed by Loss of the Second Allele. Cell Cycle, 2005. 4(12): p. 1847-1853.
15. Lee, V.D. and B. Huang, Missense mutations at lysine 350 in beta 2-tubulin confer altered sensitivity to microtubule inhibitors in Chlamydomonas. The Plant Cell, 1990. 2(11): p. 1051-1057.
16. Gupta Jr., M.L., et al., Mutagenesis of β-tubulin cysteine residues in Saccharomyces cerevisiae: Mutation of cysteine 354 results in cold-stable microtubules. Cell Motility, 2001. 49(2): p. 67-77.
17. Gupta, M.L., et al., β-Tubulin C354 Mutations that Severely Decrease Microtubule Dynamics Do Not Prevent Nuclear Migration in Yeast. Molecular Biology of the Cell, 2002. 13(8): p. 2919-2932.
18. Flynn, B.L., et al., Discovery of 7-Hydroxy-6-methoxy-2-methyl-3-(3,4,5-trimethoxybenzoyl)benzo[b]furan (BNC105), a Tubulin Polymerization Inhibitor with Potent Antiproliferative and Tumor Vascular Disrupting Properties. Journal of Medicinal Chemistry, 2011. 54(17): p. 6014-6027.
19. Sun, Q., et al., PySCF: the Python-based simulations of chemistry framework. Wiley Interdisciplinary Reviews: Computational Molecular Science, 2018. 8(1): p. e1340.
20. Mei, Y., et al., LibSC: Library for scaling correction methods in density functional theory. Journal of chemical theory and computation, 2022. 18(2): p. 840-850.
21. Shao, X., et al., Machine learning electronic structure methods based on the one-electron reduced density matrix. Nature Communications, 2023. 14(1): p. 6281.
22. Povedano, J.M., et al., A Multipronged Approach Establishes Covalent Modification of β-Tubulin as the Mode of Action of Benzamide Anti-cancer Toxins. Journal of Medicinal Chemistry, 2020. 63(22): p. 14054-14066.
23. Courbet, A., et al., Imidazoquinoxaline anticancer derivatives and imiquimod interact with tubulin: Characterization of molecular microtubule inhibiting mechanisms in correlation with cytotoxicity. PLOS ONE, 2017. 12(8): p. e0182022.

24. Yang, J., et al., Cevipabulin-tubulin complex reveals a novel agent binding site on α-tubulin with tubulin degradation effect. Science Advances, 2021. 7(21): p. eabg4168.
25. DSNBK, P., S.R. Atla, and R.P. Atla, In vitro Anthelmintic activity of Aralia racemosa. L (root) and Argyreia Pilosa Wight & Arn.(Whole plant) against Pheretima Posthuma: In-vitro Anthelmintic Potential of Aralia racemosa. L and Argyreia pilosa Wight & Arn. Iranian Journal of Pharmaceutical Sciences, 2021. 17(3): p. 23-32.
26. DSNBK, P., et al., Anthelmintic activity of Manosa alliacea against Pheretima posthuma: Invitro and Insilico approach. Thai Journal of Pharmaceutical Sciences (TJPS), 2020. 44(3).
27. DSNBK, P., et al., Insilico and Invitro anthelmintic properties of phytocompounds in Rostellularia quinquangularis (J. Koenig ex Roxb.) Nees. Iranian Journal of Pharmaceutical Sciences, 2023. 19(2): p. 110-123.
28. Prasanth, D., et al., In silico screening of plant-derived anti-virals from Shorea hemsleyana (King) king ex Foxw against SARS CoV-2 main protease. Chemistry Africa, 2023. 6(1): p. 345-366.
29. Prasanth, D.S., et al., Citronellal as a promising candidate for Alzheimer's disease treatment: A comprehensive study on in silico and in vivo anti-acetylcholine esterase activity. Metabolites, 2023. 13(11): p. 1133.
30. Cheng, F., et al., admetSAR: a comprehensive source and free tool for assessment of chemical ADMET properties. 2012, ACS Publications.
31. Banerjee, P., et al., ProTox-II: a webserver for the prediction of toxicity of chemicals. Nucleic acids research, 2018. 46(W1): p. W257-W263.
32. Argaman, N. and G. Makov, Density functional theory: An introduction. American Journal of Physics, 2000. 68(1): p. 69-79.
33. Han, D., et al., Integrating Electronic Structure Theory Calculations with Python and Cheminformatics Tools. 2025, ACS Publications.
34. Lykhin, A.O., et al., Dipole Moments and Transition Dipole Moments Calculated by Pair-Density Functional Theory with State Interaction. The Journal of Physical Chemistry A, 2023. 127(18): p. 4194-4205.
35. Li, C. and G.K.-L. Chan, Accurate QM/MM molecular dynamics for periodic systems in GPU4PySCF with applications to enzyme catalysis. Journal of Chemical Theory and Computation, 2025. 21(2): p. 803-816.
36. Prasanth, D.S.N.B.K., et al., In vitro Anthelmintic Impact of Various Extracts of Pavetta tomentosa Root on Pheretima posthuma and in-silico Molecular Docking Evaluation of some Isolated phytoconstituents. Indian J. Pharm. Educ. Res, 2020. 54(2): p. S251-S260.
37. Trott, O. and A.J. Olson, AutoDock Vina: improving the speed and accuracy of docking with a new scoring function, efficient optimization, and multithreading. Journal of computational chemistry, 2010. 31(2): p. 455-461.
38. Gangadharappa, B.S., et al., Structural insights of metallo-beta-lactamase revealed an effective way of inhibition of enzyme by natural inhibitors. J Biomol Struct Dyn, 2020. 38(13): p. 3757-3771.
39. Lemenkova, P., Python libraries matplotlib, seaborn and pandas for visualization geospatial datasets generated by QGIS. Analele stiintifice ale Universitatii" Alexandru Ioan Cuza" din Iasi-seria Geografie, 2020. 1: p. 13-32.
40. Sial, A.H., S.Y.S. Rashdi, and A.H. Khan, Comparative analysis of data visualization libraries Matplotlib and Seaborn in Python. International Journal, 2021. 10(1): p. 277-281.
41. Jamkhande, P.G., et al., In vitro anthelmintic efficacy of Borassus flabellifer Linn. (Palmae) against Pheretima posthuma. Asian Pac. J. Trop. Dis., 2014. 4: p. S199-S203.
42. Chen, J., et al., Global burden of soil-transmitted helminth infections, 1990-2021. Infect Dis Poverty, 2024. 13(1): p. 77.
43. Montresor, A., et al., The global progress of soil-transmitted helminthiases control in 2020 and World Health Organization targets for 2030. PLOS Neglected Tropical Diseases, 2020. 14(8): p. e0008505.
44. Wu, J., et al., A narrative review: The pharmaceutical evolution of phenolic syringaldehyde. Biomedicine & Pharmacotherapy, 2022. 153: p. 113339.
45. Kapinder, N. Daram, and A.K. Verma, Drug resistance in helminth parasites: Role of plant-based natural therapeutics, in Natural Product Based Drug Discovery Against Human Parasites: Opportunities and Challenges. 2023, Springer. p. 553-579.
46. Zochedh, A., et al., Experimental and computational evaluation of syringic acid–structural, spectroscopic, biological activity and docking simulation. Polycyclic Aromatic Compounds, 2023. 43(7): p. 6516-6548.
47. Adeyi, O.E., et al., Syringic acid demonstrates better anti-apoptotic, anti-inflammatory and antioxidative ef*fects than ascorbic acid via maintenance of the endogenous antioxidants and downregulation of pro-inflammatory and apoptotic markers in DMN-induced hepatotoxicity in rats.* Biochemistry and Biophysics Reports, 2023. **33**: p. 101428.